

Article

Laser-Induced Exothermic Bonding of SiCp/Al Composites with Nanostructured Al/Ni Energetic Interlayer

Guangjie Feng^{1,2,*}, Bingxu Hu¹, Xiaojian Liu³, Yan Wei¹, Zhuoran Li², Peng He², Zhiliang Cheng^{4,*}, Yifeng Wang¹, Dean Deng¹ and Xiuxia Yang^{5,*}

¹ College of Materials Science and Engineering, Chongqing University, Chongqing 400044, China; 202009021009@cqu.edu.cn (B.H.); 201909131163@cqu.edu.cn (Y.W.); wangyf0902@cqu.edu.cn (Y.W.); deandeng@cqu.edu.cn (D.D.)

² State Key Laboratory of Advanced Welding and Joining, Harbin Institute of Technology, Harbin 150001, China; lizr@hit.edu.cn (Z.L.); hepenghit@hit.edu.cn (P.H.)

³ Beijing Institute of Control Engineering, Beijing 100080, China; 14b309026@hit.edu.cn

⁴ School of Chemistry and Chemical Engineering, Chongqing University of Technology, Chongqing 400054, China

⁵ College of Land Resources and Environment, Jiangxi Agricultural University, Nanchang 330045, China

* Correspondence: fenggj@cqu.edu.cn (G.F.); purper@cqu.edu.cn (Z.C.); 13b909095@hit.edu.cn (X.Y.)

Abstract: In this study, SiCp/Al composites were bonded using the laser-induced exothermic bonding method. The nanostructured Al/Ni energetic materials were prepared by the high-energy ball-milling method and served as the bonding interlayer. The joint microstructure was characterized by SEM, EDS, TEM, and XRD. The effect of Zr content on the joint microstructure and shear strength was investigated. The results indicated that after the ball-milling process the Al and Ni particles underwent strong plastic deformations and were welded to each other, forming the nanostructured Al/Ni energetic materials with a lamellar structure. Compared with the raw powders, the location of the exothermic peak decreased by 42 K, and its exothermic performance was significantly improved. The exothermic reactions that occurred in the Al/Ni interlayer provided the required heat for the bonding process. Near the bonding interface, the interlayer could not react completely due to the cooling effect of the substrates, forming a mixture of residual metal particles and Ni-Al compounds. The addition of Zr content enhanced the interfacial reactions between the bonding interlayer and the SiCp/Al composites. The interlayer products transformed from NiAl to the eutectic organization of NiAl + Ni-Al-Zr, thus decreasing the pores in the joint and improving the bonding quality. With an increase in the Zr content, the joint shear strength first increased and then decreased. When the Zr content was 10 wt.%, the joint shear strength reached a maximum of 22 MPa.

Keywords: SiCp/Al composites; exothermic bonding; nanostructured energetic materials; microstructure; mechanical property



Citation: Feng, G.; Hu, B.; Liu, X.; Wei, Y.; Li, Z.; He, P.; Cheng, Z.; Wang, Y.; Deng, D.; Yang, X.

Laser-Induced Exothermic Bonding of SiCp/Al Composites with Nanostructured Al/Ni Energetic Interlayer. *Crystals* **2022**, *12*, 938. <https://doi.org/10.3390/cryst12070938>

Academic Editors: Wenwu Xu, Fawei Tang and Massoud Malaki

Received: 8 June 2022

Accepted: 28 June 2022

Published: 3 July 2022

Publisher's Note: MDPI stays neutral with regard to jurisdictional claims in published maps and institutional affiliations.



Copyright: © 2022 by the authors. Licensee MDPI, Basel, Switzerland. This article is an open access article distributed under the terms and conditions of the Creative Commons Attribution (CC BY) license (<https://creativecommons.org/licenses/by/4.0/>).

1. Introduction

Silicon carbide particle reinforced aluminum matrix composites (SiCp/Al composites), which are composed of silicon carbide particles and aluminum alloy matrix, are typical metal matrix composites [1–4]. Due to the advantages of high specific strength, good wear resistance, and a low thermal expansion coefficient, SiCp/Al composites have been widely used in electronics, aerospace, and other fields [5–7]. However, SiCp/Al composites have poor machinability and are difficult to use in manufacturing large or complex components [8]. Assembling modular SiCp/Al composite parts by welding can break through the limitations of component size and structure, thus significantly broadening their application and achieving huge economic benefits [9,10]. However, due to the huge difference in physical and chemical properties between the SiC particle and the Al matrix, the welding

of SiCp/Al composites is difficult [11]. At present, this problem has not been overcome and has become one of the main obstacles to the further application of SiCp/Al composites.

The welding of SiCp/Al composites has three difficulties. The first one is the harmful interfacial reactions between the SiC particle and the aluminum matrix. If exposed to high temperatures for a long time, excess interfacial reactions occur, forming a large amount of brittle compound Al_4C_3 and deteriorating the performance of the composites and joint [12]. The second problem is the weak bonding between the SiC particle and the filler metal due to the high chemical inertness of SiC particles. The third is the oxide film on the surface of the aluminum matrix, which hinders the atomic interdiffusion at the bonding interface and leads to weak bonding [13]. Using chemical or mechanical methods [14], the oxide film can be removed before the welding process. Thus, the main problem in welding SiCp/Al composites is how to avoid the harmful interfacial reactions within the composites and simultaneously promote the metallurgical reaction between the SiC particles and the filler metals. To solve this problem, the interfacial reactions between the SiC particle, aluminum matrix, and filler metal should be precisely controlled. Due to the limitation of heating methods, conventional welding methods cannot meet the above requirements, and a new welding method must be developed.

Exothermic bonding technology has attracted a lot of attention. It utilizes the self-propagating high-temperature synthesis (SHS) reaction of an exothermic interlayer as the heat source to heat the bonding interface and enhance the metallurgical reactions [15–17]. During the exothermic bonding process, the SHS reaction can quickly heat a narrow area near the bonding interface to a high temperature and improve the atomic activity, while the rest area is kept at a low temperature [18]. Thus, thermal damage to the base materials can be avoided. Great efforts have been made on this topic. Materials such as superalloy [19], TiB_2/Ni cermet [20], SiC ceramic [21], C_f/Al composites [22], and TiAl intermetallics [23] have been joined using the exothermic bonding technology. Although some results have been achieved, the main problems have not been solved. In the reported research, the exothermic bonding process is realized using the powder interlayer [24] or nano-multilayer [25]. When using the powder interlayer, the high ignition temperature harms the base materials. When using a nano-multilayer, a large bonding pressure is required, which may lead to damage to the base materials. In addition, the fabrication of nano-multilayers has a high cost. To overcome the above problem, the ideal solution is to fabricate an exothermic interlayer that processes the combined advantages. Therefore, the research must be conducted from a new perspective in the interdisciplinary study of energetic materials and welding.

As fundamental research, this paper aims to solve the bonding problem of the SiCp/Al composites from the viewpoint of interdisciplinary research. The nanostructured energetic materials were fabricated and acted as the exothermic interlayer. The SiCp/Al composites were bonded via the laser-induced exothermic bonding method. The exothermic properties of the exothermic interlayer and the joint microstructure were characterized. The effect of Zr addition on the joint microstructures and mechanical properties was investigated.

2. Materials and Methods

The volume fraction of the SiC particles in the SiCp/Al composites was 50%. The matrix of the SiCp/Al composites was the 6061 aluminum alloy. Figure 1 shows the microstructure of the SiCp/Al composites. Before the exothermic bonding, the SiCp/Al composites were cut into $5\text{ mm} \times 5\text{ mm} \times 4\text{ mm}$ and $12\text{ mm} \times 8\text{ mm} \times 2\text{ mm}$ specimens. The bonding surfaces were polished using the diamond sanding discs up to grit 1000. Then, the SiCp/Al composite specimens were cleaned in acetone for 15 min with the assistance of an ultrasonic instrument.

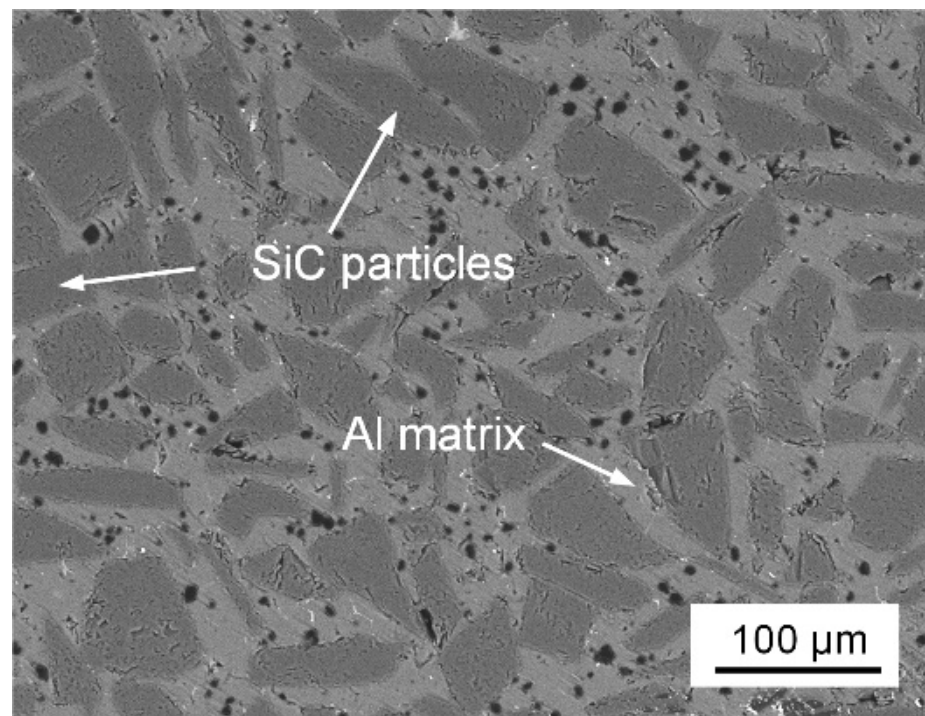


Figure 1. Microstructure of SiCp/Al composites.

Commercial Ni (500 mesh, purity 99.8%), Al (500 mesh, purity 99.7%), and Zr (500 mesh, purity 99.5%) powders were used as the raw materials to fabricate the exothermic interlayer. Then, 10 g equimolar Al and Ni powders were weighed and placed in an agate milling jar (100 mL). Zirconia balls ($\Phi 10$ mm, $\Phi 5$ mm) were used as the milling media. To protect the mixtures from reaction, oxidation, and agglomeration, 20 mL of hexane was added to the milling jar as a process-controlling agent. The ball to powder mass ratio was 10:1, and the milling time was 40 min. The rotational speed was 600 rpm. During the ball-milling process, the milling balls collided with powders and the milling jar. Thus, the milling process produced a lot of heat and increased the temperature of the powders. To prevent the possible effect of the produced heat on the products, the ball-milling process had a 15 min rest for every 5 min increment to ensure that the produced heat was fully dissipated. After the milling process, the Al and Ni particles underwent strong plastic deformations and were welded to each other, forming the nanostructured Al/Ni energetic materials. To investigate the effect of Zr addition on the bonding of SiCp/Al composites, the prepared Al/Ni materials were further milled with the Zr powders for 5 min, forming the Al/Ni/Zr energetic materials. Then, 0.5 g of the Al/Ni or Al/Ni/Zr energetic materials was cold-pressed into a compact under a pressure of 50 kN and served as the exothermic interlayer. The diameter and height of the powder compact were about 10 mm and 1.3 mm, respectively.

The laser-induced exothermic bonding of SiCp/Al composites was conducted under the protection of argon to avoid the adverse effect of oxygen. The joining schematic diagram is represented in Figure 2. During the bonding, the exothermic interlayer was applied between the SiCp/Al composites. A laser beam (YAG-W100E, P = 200 W, Han's Laser Technology Industry Group Co., Ltd., Shenzhen, China) heated and ignited the interlayer. Then, the combustion flame propagated to the other side and finished the bonding process.

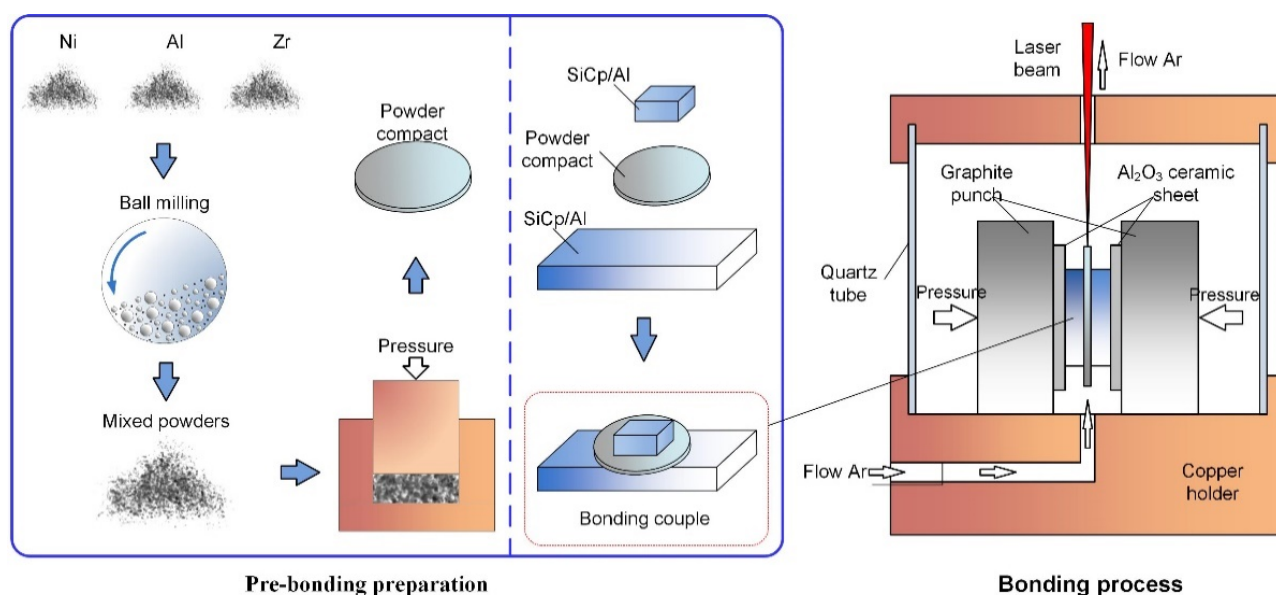


Figure 2. Schematic diagram of laser-induced exothermic bonding.

The fabricated Al/Ni energetic materials were characterized by scanning electron microscopy (SEM, FEI Nova400, FEI Company, Hillsboro, OR, USA), transmission electron microscopy (TEM, Talos F200X, FEI Co., Ltd., Hillsboro, OR, USA), X-ray diffraction (XRD, D8 ADVANCE, Bruker Company, Karlsruhe, Germany), and differential scanning calorimetry (DSC, NETZSCH STA449C, Erich NETZSCH GmbH & Co. Holding KG, Selb, Germany) to examine their microstructure and exothermic properties. The joint microstructure was characterized by a scanning electron microscope (SEM, FEI Nova400, FEI Company, Hillsboro, OR, USA) equipped with an energy-dispersive spectrometer (EDS, FEI Company, Hillsboro, OR, USA) and X-ray diffraction (XRD, D8 ADVANCE, Bruker Company, Karlsruhe, Germany). The shear test was conducted on the joint to evaluate the mechanical properties using a universal testing machine (INSTRON 5569, Instron Corporation, Norwood, MA, USA) at a shear rate of $0.5 \text{ mm} \cdot \text{min}^{-1}$.

3. Results and Discussion

3.1. Nanostructured Al/Ni Energetic Interlayer

In this study, the bonding of SiCp/Al composites was realized with the assistance of the laser-induced exothermic reaction in the interlayer, which provided all the energy required for the atomic interdiffusion and metallurgical reactions. Thus, the exothermic properties of the interlayer determined the bonding quality. Up to now, many exothermic reaction systems have been studied, such as Al-Ni [26], Al-Ti [25], Ti-Al-B [27], and Ti-Al-C [28]. According to our previous study [29,30], the equimolar Al-Ni system possessed a low reaction activation energy, high exothermicity, and combustion stability. The adiabatic temperature of the equimolar Al-Ni system was as high as 1912 K [31], which could provide enough energy for the bonding process. Thus, this study selected the equimolar Al-Ni system to fabricate the exothermic interlayer and bond the SiCp/Al composites.

Mukasyan et al. [32] reported that the high-energy ball-milling treatment could refine the structure of the energetic materials. The fine structure can significantly decrease the ignition temperature and increase the activity of the Al/Ni composites, which is beneficial to the exothermic bonding of the SiCp/Al composites. Figure 3 shows the microstructure of the Al/Ni composites before and after the high-energy ball-milling treatment. It can be seen from the figure that the high-energy ball-milling treatment greatly changed the morphology and distribution of the Al and Ni powders. The raw powders in Figure 3a presented a spherical shape. Some particles aggregated together. After the ball-milling treatment, a large deformation occurred in the particles, forming the Al/Ni composite particles. Within

the Al/Ni composite particle, a clear lamellar structure was observed. The white and dark-gray layers were Ni and Al, respectively. To examine the effect of the ball-milling process on the Al/Ni interface, the TEM analysis was employed. Figure 4 shows the TEM figure of the Al/Ni composite particle. The lamellar structure was clear. The thicknesses of the Ni and Al layers ranged from 50 nm to 200 nm. To discover more details, the Al/Ni interface was enlarged. The corresponding elemental mapping figure indicated the Al/Ni interface was sharp. Only a narrow Al-Ni mixed zone was detected, which meant that no chemical reactions occurred between the Al and Ni. Figure 5 shows the XRD results of the Al/Ni powders before and after the ball-milling treatment. Only Ni and Al peaks were detected in the curves. It should be noted that after the ball-milling treatment, the locations of the peaks shifted slightly to the left, which was due to the refinement of the materials.

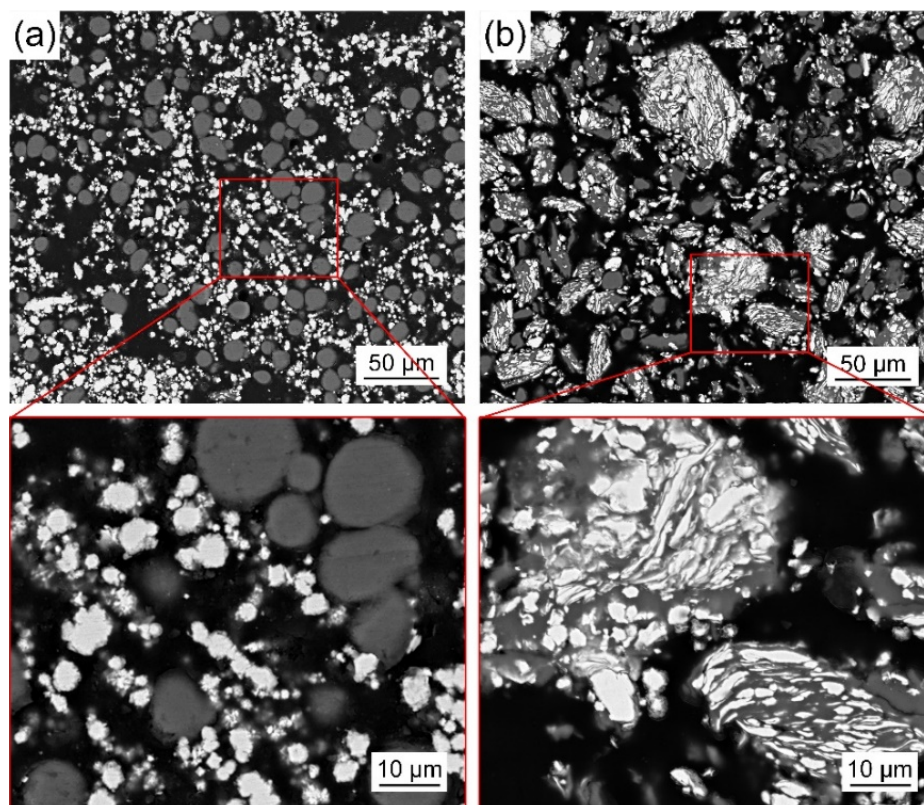


Figure 3. Microstructure of Al/Ni energetic composites (a) before and (b) after ball milling.

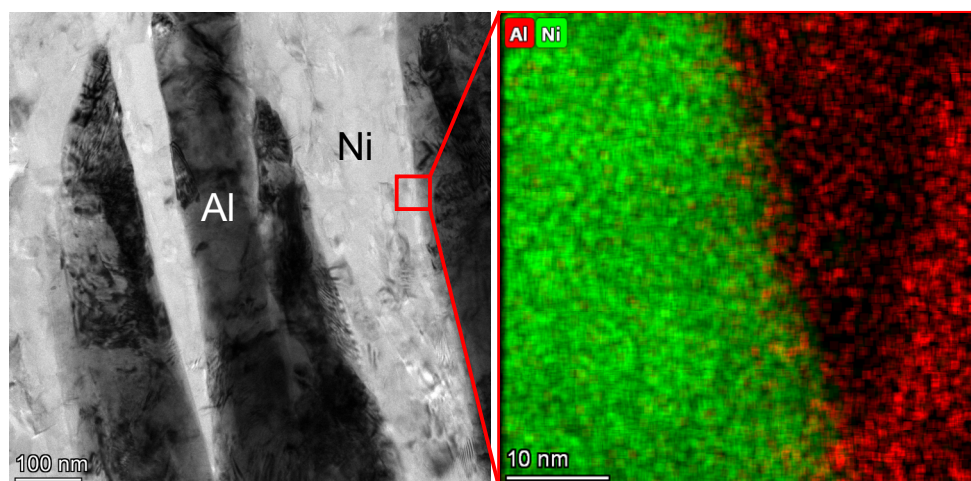


Figure 4. TEM figure of the nanostructured Al/Ni energetic composites.

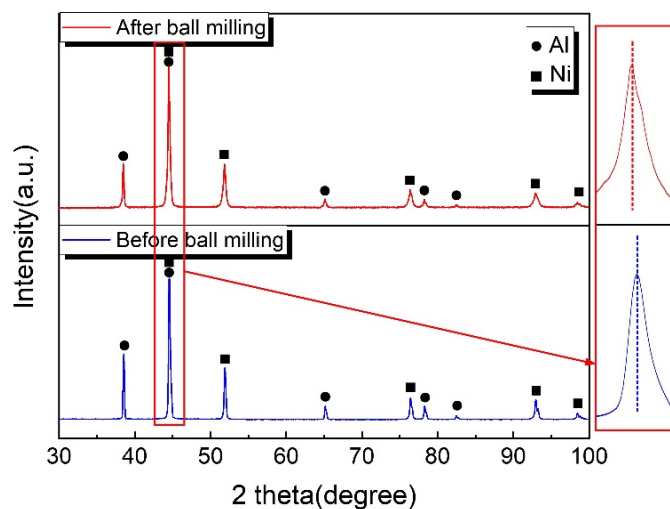


Figure 5. XRD results of the Al/Ni energetic composites.

The above analysis indicated that after the ball-milling treatment the Al-Ni mixed powders transformed into the nanostructured Al/Ni composites. In general, the refinement of the structure in the Al/Ni composites was beneficial to the exothermic properties of the materials [33]. This was because, during the reaction, the fine lamellar structure decreased the atomic diffusion distance and increased the reaction rate [34]. Compared with the original mixed powders, the fabricated nanostructured Al/Ni energetic materials not only had a fine lamellar structure but also had a uniform distribution of the Al and Ni, which all made the exothermic reactions occur more easily. Figure 6 shows the DSC curves of the Al/Ni energetic composites. There were two exothermic peaks in the DSC curves. The first peak was the main exothermic peak, which was due to the solid-state diffusion between the Al and Ni. After the ball-milling treatment, the location of the first peak shifted to a low temperature. The decrease in the peak location was about 42 K. This phenomenon was caused by the refinement of the structure. At low temperatures, the solid-state diffusion between the Al and Ni was enhanced due to the formation of the nanostructure. The second peak was due to the melting of the Al. After the ball-milling treatment, the location of the second peak did not change. The change in the main exothermic peak location meant that the fabricated nanostructured Al/Ni energetic materials had a high activity, which may be beneficial to the bonding process.

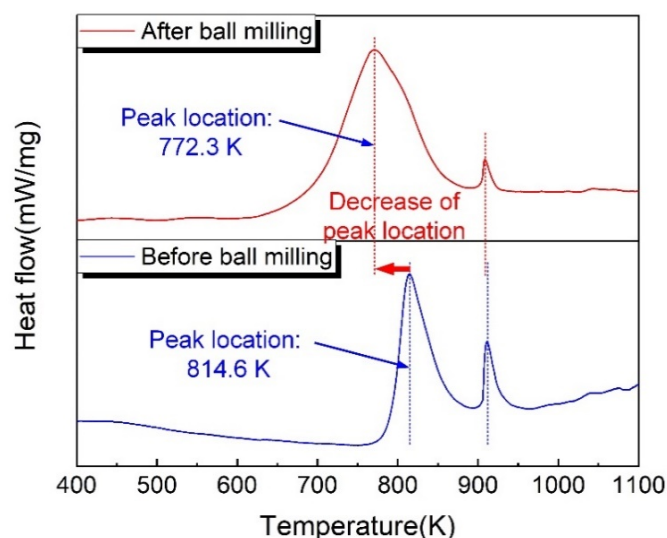


Figure 6. DSC curves of the Al/Ni energetic composites.

3.2. Joint Microstructure

The Al/Ni nanostructured energetic materials were cold-pressed into a powder compact and served as the exothermic interlayer to bond the SiCp/Al composites. Figure 7 shows the microstructure of the joint bonded under a pressure of 4 MPa. After being ignited by the laser beam, the SHS reaction occurred. The interlayer products bonded well with the SiCp/Al composites. Due to the particularity of the SHS reaction, some pores were unavoidably formed in the joint. To discover more details, the zones in the interlayer products and near the bonding interface were enlarged. Figure 7b shows the microstructure of the interlayer products in the joint center. It indicates that the Al/Ni interlayer reacted completely, forming the white-gray products (Position A). Unlike the morphology in Figure 7b, the interlayer products near the bonding interface demonstrated a different morphology. The exothermic reactions near the bonding interface were incomplete, forming a mixture of bright phase (Position C), off-white phase (Position D), and light-gray phase (Position E). The incomplete reactions were mainly due to the cooling effect of the SiCp/Al composites, which absorbed the reaction heat and partially quenched the SHS reaction. In the SiCp/Al composites near the bonding interface, some light-gray phases (Position B) were also produced. An EDS analysis was performed on each region of the joint. The analysis results in Table 1 show that the phases in the interlayer products consisted of Ni and Al. According to their Ni/Al ratios, the white-gray phase (Position A), bright phase (Position C), off-white phase (Position D) and light gray phase (Position E) were supposed to be NiAl, Ni-rich Ni_3Al , Ni_2Al_3 , and NiAl_3 , respectively. The light-gray phase in the SiCp/Al composites was confirmed to be NiAl_3 , which was formed due to the diffusion of Ni. The gray phase (Position F) was the melted aluminum matrix. To further identify the phase composition of the joint, the XRD test was carried out on the interlayer products. The results in Figure 8 indicate that the interlayer products were a mixture of the Ni, Al, NiAl_3 , Ni_2Al_3 , Ni_3Al , and NiAl, which proved the above expectation.

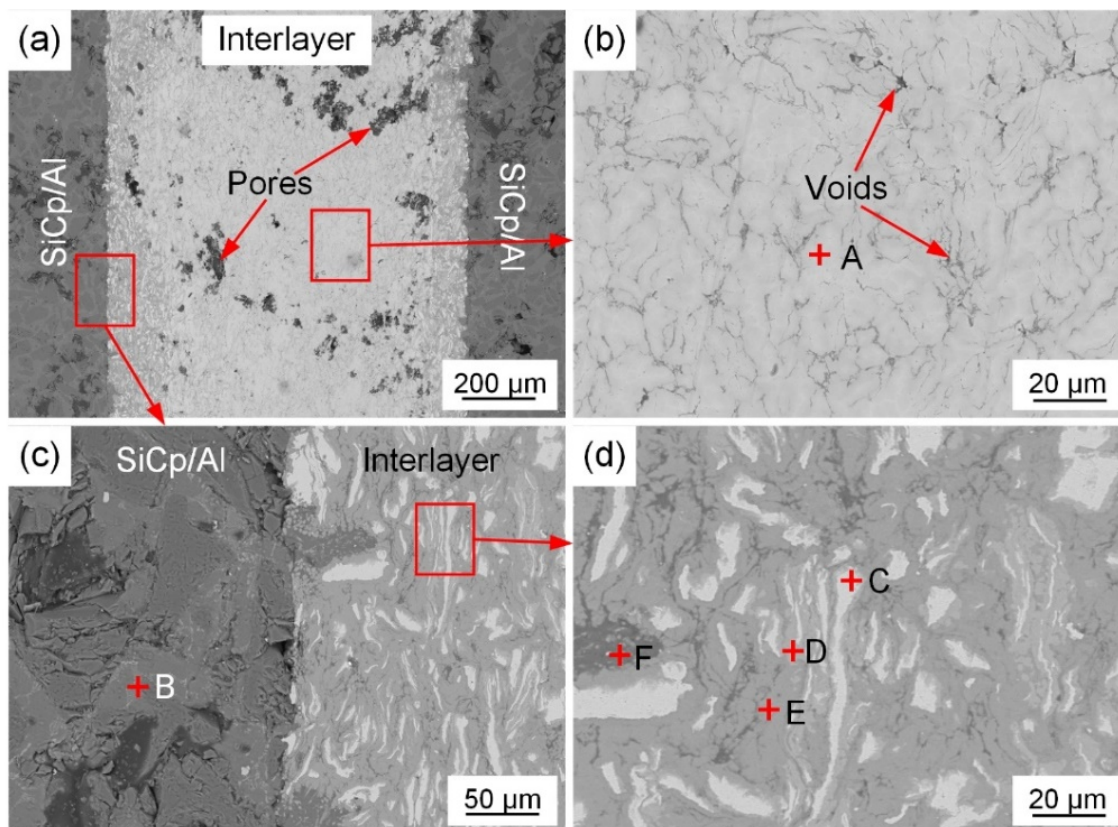
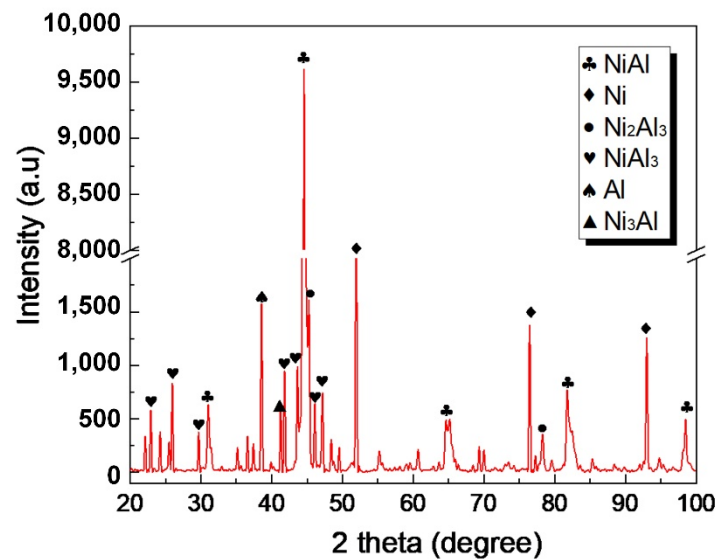


Figure 7. Microstructure of the joint bonded with Al/Ni interlayer (4 MPa). (a) Overall joint; (b) joint center; (c) bonding interface; (d) enlargement of zone in (c).

Table 1. EDS analysis results of each position in Figure 7 (at.%).

Position	Al	Ni	Si	Possible Phase
A	44.5	55.5	-	NiAl
B	71.3	21.1	4.6	NiAl ₃
C	79.1	16.0	4.9	Ni-rich Ni ₃ Al
D	65.2	34.8	-	Ni ₂ Al ₃
E	72.6	23.7	3.7	NiAl ₃
F	99.1	0.9	-	Al

**Figure 8.** XRD results of Al/Ni interlayer products.

The SiCp/Al composites bonded in this paper had a high volume fraction of the SiC particles. Previous research [35] indicated that the SiC ceramic had a high melting point and low chemical affinity with Ni-Al intermetallics due to the high stability of the Si-C ionic bond. To increase the chemical affinity between the SiC ceramic and filler metals, active elements such as Ti or Zr were often added in the filler metals. The previous research by our group [22] indicated that the addition of Zr in the Ni-Al system could transform the interlayer products from NiAl to the eutectic mixture of NiAl + Ni-Al-Zr. The formation of eutectic products was beneficial to the densification of the interlayer products. Thus, to improve the bonding quality of the SiCp/Al composites, Zr was mixed with the fabricated Al/Ni nanostructured energetic materials, forming the Al/Ni/Zr exothermic interlayer. During the exothermic reaction, the added Zr absorbed heat, thus decreasing the released heat. In order to ensure the exothermic reaction is self-sustaining, the content of Zr should be lower than 36.08%.

Figure 9 shows the microstructure of the joint bonded with the Al/Ni/Zr interlayer. It can be seen that the addition of Zr improved the bonding quality. Compared with the joint in Figure 7, the pores and the cracks were obviously reduced. This was mainly because the Zr addition transformed the interlayer products from Ni-Al to the eutectic mixture of NiAl + Ni-Al-Zr. The eutectic products had a lower melting point than the NiAl, thus prolonging the existence of the liquid phase. Under the effect of bonding pressure, the interlayer products could be densified more easily, leading to a decrease in the pores and cracks in the joint. To detect more details, different zones in the joint were enlarged. Figure 9b,c show the microstructures at the bonding interface. It can be seen in the figures that the interlayer products bonded well with the SiCp/Al composites. However, the interlayer products on the two sides were different. The interlayer products in Figure 9b were a mixture of bright phase (Position A), light-gray phase (Position B), gray phase (Position C), and dark-gray phase (Position D), while the interlayer products in Figure 9c

were the same as the interlayer products in Figure 9d. This phenomenon was mainly due to the different heat transfer conditions on the two sides. As introduced in Section 2, the dimensions of the SiCp/Al pieces were different. The SiCp/Al composites in Figure 9b were larger than those in Figure 9c, thus absorbing more heat. The SHS reaction was quenched, forming the unreacted products on this side.

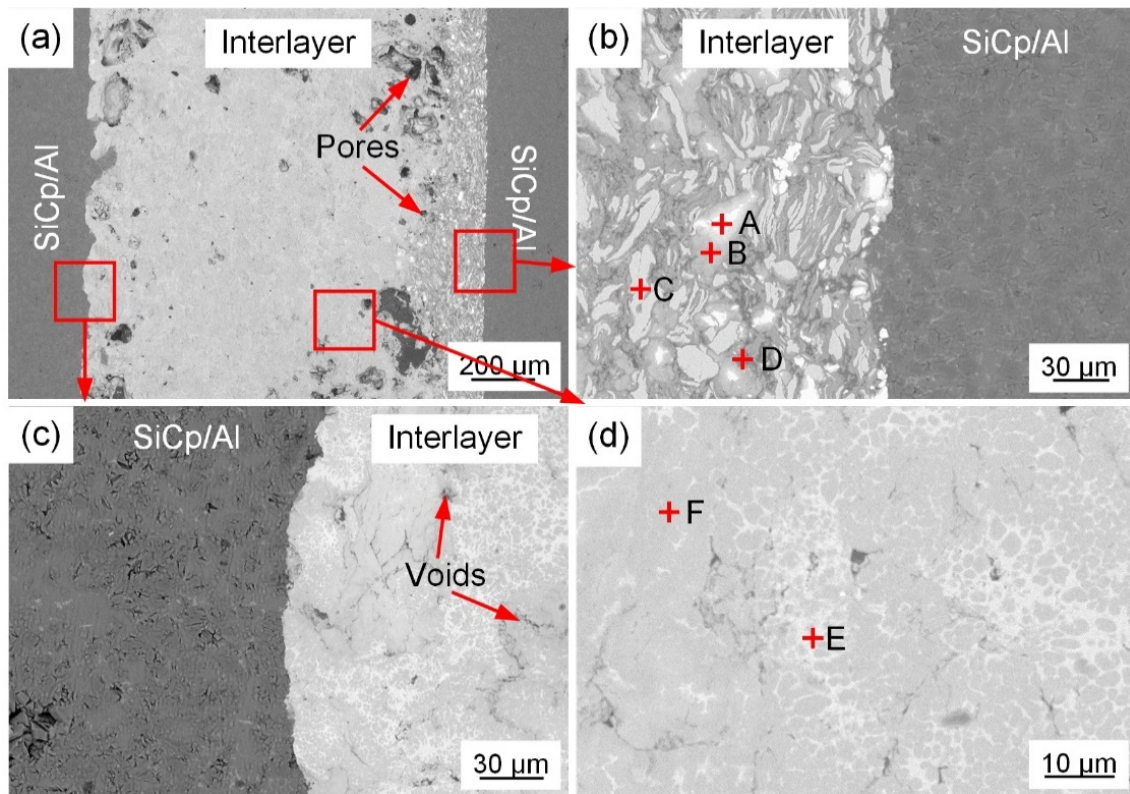


Figure 9. Microstructure of joint bonded with Al/Ni/Zr interlayer (10 wt.% Zr). (a) Overall joint; (b) interface on right side; (c) interface on left side; (d) joint center.

An EDS analysis was performed on each region of the joint, and the results are shown in Table 2. According to the chemical composition and Ni-Al-Zr phase diagram, the bright phase (Position A), light-gray phase (Position B), and dark-gray phase (Position D) were confirmed to be Ni-Al-Zr ternary compounds. The gray phase (Position C) was confirmed to be Ni_3Al . The interlayer products were composed of a network-like white phase E and an off-white phase F. According to the EDS results, the white phase E mainly contained Ni, Al, and Zr and was speculated to be the Ni-Al-Zr ternary compound. The off-white phase F was confirmed to the Al-rich NiAl, according to our previous research [22]. An XRD analysis was conducted on the interlayer products. The results in Figure 10 indicate that the NiAl, Ni_3Al , NiAl_3 , and Ni-Al-Zr ternary compounds were detected.

Table 2. EDS analysis results of each position in Figure 9 (at.%).

Position	Al	Ni	Zr	Si	Possible Phase
A	17.2	6.8	76.0	-	Ni-Al-Zr
B	28.3	6.6	62.4	2.7	Ni-Al-Zr
C	21.0	73.1	-	5.9	Ni_3Al
D	74.4	9.2	14.2	2.3	Ni-Al-Zr
E	40.1	43.5	16.4	-	Ni-Al-Zr
F	57.0	43.0	-	-	NiAl

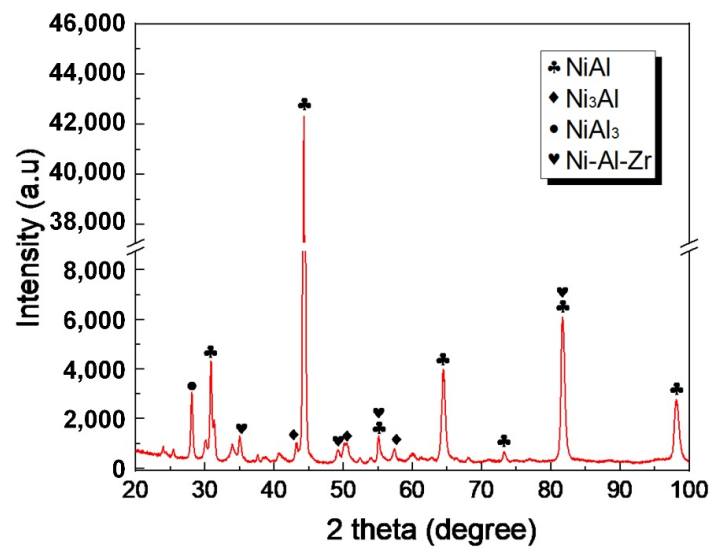


Figure 10. XRD results of Al/Ni/Zr interlayer products.

3.3. Effect of Zr Content on Joint Microstructure and Shear Strength

Figure 11 shows the microstructures of the joints bonded using the Al/Ni/Zr interlayer with different Zr contents. It can be seen that the Zr content significantly influenced the joint microstructure. The changes in the joint microstructure were mainly manifested in two aspects, which were the quantity of pores and the reaction degree of the bonding interlayer. With an increase in Zr content, the size and the quantity of pores decreased gradually. Meanwhile, the fraction of the incompletely reacted interlayer increased. When the Zr content was 5 wt.%, the interlayer reacted completely after being ignited by the laser beam. Many large pores formed in the interlayer products and at the bonding interfaces. With an increase in Zr content, the incompletely reacted region in the interlayer gradually increased, and the size and quantity of the pores decreased noticeably. When the Zr was 15 wt.%, the incompletely reacted region in the interlayer extended to the entire interlayer. The pores were small and dispersed in the interlayer products. With a further increase in the Zr content, the joint microstructure did not change, except for the increasing volume fraction of the residual Zr particles.

The above phenomenon was mainly because the Zr content changed the phase composition of the interlayer products and the release of heat. The previous study [36] indicated that the equimolar Ni-Al reaction system had an adiabatic temperature of 1912 K, which was the melting point of NiAl. During the exothermic reaction, the interlayer products were in a solid–liquid coexistence state. The molar fraction of the liquid in the interlayer products was 42%. According to the analysis in Section 3.2, the addition of Zr transformed the interlayer products from NiAl to the eutectic NiAl + Ni-Al-Zr. Compared with NiAl, the eutectic NiAl + Ni-Al-Zr decreased the melting point of the interlayer products, which also increased the volume fraction of the liquid phase in the interlayer products. During the bonding process, there was more time to densify the interlayer products before their solidification. Under the bonding pressure, the interlayer products were squeezed by the SiCp/Al composites. Thus, it was much easier to eliminate the original pores in the interlayer. The size and quantity of pores decreased with an increase in the Zr content. However, the addition of Zr decreased the released heat. During the bonding process, the SiCp/Al composites absorbed the reaction heat from the interlayer, which had a quenching effect on the interlayer. With an increase in the Zr content, the amount of released heat decreased gradually. The region near the SiCp/Al composites could not react completely due to the heat loss to the substrate. When the Zr content was 15 wt.% or higher, the incompletely reacted region extended to the entire interlayer. The white residual Zr particles dispersed in the interlayer.

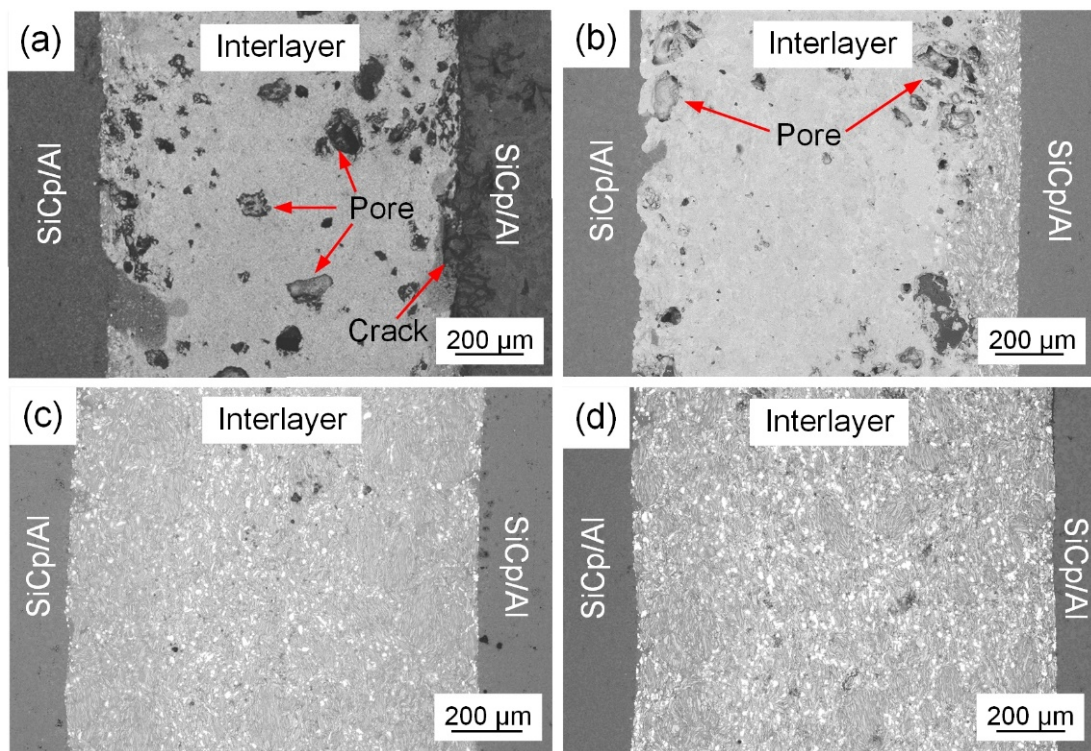


Figure 11. Microstructure of joints bonded using interlayers with different Zr contents. (a) 5 wt.%; (b) 10 wt.%; (c) 15 wt.%; (d) 20 wt.%.

Figure 12 shows the influence of Zr content on the joint shear strength. The Zr content influenced the joint microstructure and defects, thus determining the joint shear strength. When the Zr content was 5 wt.%, many large pores formed in the joint, and the micro-cracks were also detected. When the Zr content increased to 10 wt.%, the size and number of pores decreased significantly. The cracks at the bonding interface disappeared. The interlayer products bonded well with the SiCp/Al composites. Thus, the joint shear strength increased to 22 MPa. The further increase in Zr content significantly decreased the exothermicity of the interlayer. The interlayer could not react completely. The residual metal particles affected the inhomogeneity of materials, and the low exothermicity of the interlayer decreased the atomic mobility at the bonding interface, leading to the weak bonding in the joint. As a result, the joint shear strength decreased dramatically.

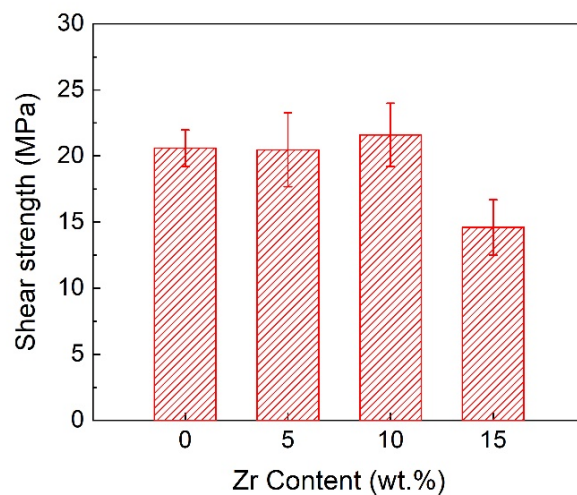


Figure 12. Effect of Zr content on joint shear strength.

Although the maximum joint shear strength was achieved when the Zr content was 10 wt.%, the joint was not satisfactory. Pores and residual metal particles were observed in the joint. There were many reasons for this phenomenon. For example, the interlayer used in this study was the powder compact that contained many original pores, the exothermicity of the interlayer was not high enough, and the densification process of the interlayer products needed to be improved. However, as fundamental research, the successful bonding of SiCp/Al composites in this study validated the feasibility and validity of the bonding method. The above problems will be further studied.

4. Conclusions

- (1) During the ball-milling process, the Al and Ni particles underwent strong plastic deformations and were welded to each other, forming the nanostructured Al/Ni energetic materials with a lamellar structure. The thicknesses of the Ni and Al layers ranged from 50 nm to 200 nm. Compared with the original powders, the location of the exothermic peak decreased by 42 K, and its exothermic performance was significantly improved.
- (2) Exothermic reactions occurred in the Al/Ni interlayer, providing the required heat for the bonding process. The NiAl products bonded well with the SiCp/Al composites. Near the bonding interface, the interlayer could not react completely due to the cooling effect of substrates, forming a mixture of residual metal particles and Ni-Al compounds.
- (3) The addition of Zr content enhanced the interfacial reactions between the bonding interlayer with the SiCp/Al composites. The interlayer products transformed from NiAl to the eutectic organization of NiAl + Ni-Al-Zr, thus decreasing the pores in the joint and improving the bonding quality. With the increase in the Zr content, the joint shear strength first increased and then decreased. When the Zr content was 10 wt.%, the joint shear strength reached a maximum of 22 MPa.

Author Contributions: Conceptualization, G.F., Z.L. and Y.W. (Yifeng Wang); methodology, G.F.; software, Y.W. (Yan Wei); validation, B.H. and Y.W. (Yan Wei); formal analysis, G.F., X.L. and Y.W. (Yan Wei); investigation, G.F. and Y.W. (Yifeng Wang); resources, B.H.; data curation, Y.W. (Yan Wei); writing—original draft preparation, G.F.; writing—review and editing, G.F. and Y.W. (Yan Wei); visualization, D.D.; supervision, P.H., Z.C., Y.W. (Yifeng Wang), D.D. and X.Y.; project administration, G.F.; funding acquisition, G.F. All authors have read and agreed to the published version of the manuscript.

Funding: This research was funded by the National Natural Science Foundation of China, grants 51905055 and 51975149, by the Natural Science Foundation of Chongqing, grant cstc2020jcyj-msxmX0115, by the Fundamental Research Funds for the Central Universities Project, grants 2020CDJLHZZ-086 and 2022CDJXY-010, and by the State Key Laboratory of Advanced Welding and Joining, grant AWJ-21M08.

Institutional Review Board Statement: Not applicable.

Informed Consent Statement: Not applicable.

Data Availability Statement: Not applicable.

Conflicts of Interest: The authors declare no conflict of interest.

References

1. Zha, H.; Feng, P.; Zhang, J.; Yu, D.; Wu, Z. Material removal mechanism in rotary ultrasonic machining of high-volume fraction SiCp/Al composites. *Int. J. Adv. Manuf. Technol.* **2018**, *97*, 2099–2109. [[CrossRef](#)]
2. Tayyebi, M.; Eghbali, B. Microstructure and mechanical properties of SiC-particle-strengthening tri-metal Al/Cu/Ni composite produced by accumulative roll bonding process. *Int. J. Miner. Metall. Mater.* **2018**, *25*, 357–364. [[CrossRef](#)]
3. Huang, J.; Tayyebi, M.; Assari, A.H. Effect of SiC particle size and severe deformation on mechanical properties and thermal conductivity of Cu/Al/Ni/SiC composite fabricated by ARB process. *J. Manuf. Process.* **2021**, *68*, 57–68. [[CrossRef](#)]
4. Avazzadeh, M.; Alizadeh, M.; Tayyebi, M. Structural, mechanical and corrosion evaluations of Cu/Zn/Al multilayered composites subjected to CARB process. *J. Alloys Compd.* **2021**, *867*, 158973. [[CrossRef](#)]

5. Xiao, J.; Li, S.; Bai, S.; Yan, J.; Xiong, D.; Tang, Y. Compression Brazing of SiCp/Al Composite Using a Semisolid Zn-Al-Cu Filler Metal Based on the Strain-Induced Melt Activation Process. *JOM* **2019**, *71*, 4931–4939. [[CrossRef](#)]
6. Moradi, M.M.; Aval, H.J.; Jamaati, R.; Amirkhanlou, S.; Ji, S. Effect of SiC nanoparticles on the microstructure and texture of friction stir welded AA2024/AA6061. *Mater. Charact.* **2019**, *152*, 169–179. [[CrossRef](#)]
7. Zhang, J.F.; Zhang, X.X.; Wang, Q.Z.; Xiao, B.L.; Ma, Z.Y. Simulations of deformation and damage processes of SiCp/Al composites during tension. *J. Mater. Sci. Technol.* **2018**, *34*, 627–634. [[CrossRef](#)]
8. Kwok, Y. Effects of pulse-impact on the welding of SiCp/Al-6061 aluminium matrix composites. *Mater. Sci. Technol.* **2017**, *33*, 2298–2304. [[CrossRef](#)]
9. Wang, P.; Xu, D.; Zhai, Y.; Niu, J. The dissimilar brazing of Kovar alloy to SiCp/Al composites using silver-based filler metal foil. *Appl. Phys. A* **2017**, *123*, 569. [[CrossRef](#)]
10. Chen, R.F.; Zhao, Y.H.; Shen, Z.X.; Dai, L.G.; Zhang, X.L.; Zhu, R. Study on the Joint Strength of SiCp/Al Metal Matrix Composite by Magnetron Sputtering Method. *Mater. Sci. Forum* **2009**, *628–629*, 569–574. [[CrossRef](#)]
11. Guo, W.; Hou, J.; Lin, T.; He, P. Joining high volume fraction SiC particle reinforced aluminum matrix composites (SiCp/Al) by low melting point stannous oxide–zinc oxide–phosphorus pentoxide glass. *Ceram. Int.* **2021**, *47*, 3955–3963. [[CrossRef](#)]
12. Wang, S.G.; Ji, X.H.; Zhao, X.Q.; Dong, N.N. Interfacial characteristics of electron beam welding joints of SiCp/Al composites. *Mater. Sci. Technol.* **2014**, *27*, 60–64. [[CrossRef](#)]
13. Gao, Z.; Yang, H.; Feng, J.; Ji, F.; Niu, J.; Brnic, J. Flux-Free Diffusion Joining of SiCp/6063 Al Matrix Composites Using Liquid Gallium with Nano-Copper Particles in Atmosphere Environment. *Nanomaterials* **2020**, *10*, 437. [[CrossRef](#)] [[PubMed](#)]
14. Ma, Z.Y.; Feng, A.H.; Chen, D.L.; Shen, J. Recent Advances in Friction Stir Welding/Processing of Aluminum Alloys: Microstructural Evolution and Mechanical Properties. *Crit. Rev. Solid State* **2018**, *43*, 269–333. [[CrossRef](#)]
15. Shteinberg, A.S.; Lin, Y.; Son, S.F.; Mukasyan, A.S. Kinetics of High Temperature Reaction in Ni-Al System: Influence of Mechanical Activation. *J. Phys. Chem. A* **2010**, *114*, 6111–6116. [[CrossRef](#)]
16. Yang, Z.; Ning, X.; Yu, X.; Tan, C.; Zhao, H.; Zhang, T.; Li, L.; Nie, Z.; Liu, Y. Energy Release Characteristics of Ni–Al–CuO Ternary Energetic Structural Material Processed by Cold Spraying. *J. Therm. Spray Technol.* **2020**, *29*, 1070–1081. [[CrossRef](#)]
17. Rogachev, A.S.; Mukasyan, A.S. Combustion of heterogeneous nanostructural systems (Review). *Combust. Explo. Shock Waves* **2010**, *46*, 243–266. [[CrossRef](#)]
18. Fiedler, T.; Belova, I.V.; Broxtermann, S.; Murch, G.E. A thermal analysis on self-propagating high temperature synthesis in joining technology. *Comp. Mater. Sci.* **2012**, *53*, 251–257. [[CrossRef](#)]
19. Shi, J.M.; Feng, J.C.; Liu, H.; Tian, X.Y.; Zhang, L.X. Vacuum brazing of the Gr/2024Al composite and TC4 alloy using AgCuTi filler alloy with Ni-Al interlayer as auxiliary heat source. *J. Alloys Compd.* **2017**, *694*, 672–681. [[CrossRef](#)]
20. Yang, Y.F.; Jiang, Q.C. Reaction behaviour, microstructure and mechanical properties of TiC-TiB₂/Ni composite fabricated by pressure assisted self-propagating high-temperature synthesis in air and vacuum. *Mater. Des.* **2013**, *49*, 123–129. [[CrossRef](#)]
21. Jimenez, C.; Mergia, K.; Lagos, M.; Yialouris, P.; Agote, I.; Liedtke, V.; Messoloras, S.; Panayiotatos, Y.; Padovano, E.; Badini, C.; et al. Joining of ceramic matrix composites to high temperature ceramics for thermal protection systems. *J. Eur. Ceram. Soc.* **2016**, *36*, 443–449. [[CrossRef](#)]
22. Feng, G.; Li, Z.; Zhou, Z.; Wang, Y. Joining of Cf/Al composites and TiAl intermetallics by laser-induced self-propagating high-temperature synthesis using the Ni-Al-Zr interlayer. *Mater. Des.* **2016**, *110*, 130–137. [[CrossRef](#)]
23. Feng, G.; Li, Z.; Jacob, R.J.; Yang, Y.; Wang, Y.; Zhou, Z.; Sekulic, D.P.; Zachariah, M.R. Laser-induced exothermic bonding of carbon fiber/Al composites and TiAl alloys. *Mater. Des.* **2017**, *126*, 197–206. [[CrossRef](#)]
24. Umbrajkar, S.M.; Seshadri, S.; Schoenitz, M.; Hoffmann, V.K.; Dreizin, E.L. Aluminum-Rich Al-MoO₃ Nanocomposite Powders Prepared by Arrested Reactive Milling. *J. Propul. Power* **2008**, *24*, 192–198. [[CrossRef](#)]
25. Ma, Y.; Li, H.; Yang, L.P.; Hu, A.M. Microstructures and Reaction Properties of Ti/Ni, Ti/Al and Ni/Al Multilayer Films. *J. Nano Res.* **2018**, *54*, 22–34. [[CrossRef](#)]
26. Liao, S.; Luo, X.; Tao, J.; Tang, B.; Guo, X.; Ding, Q. Microstructure and reaction properties of Ni/Al micro-nano composites produced by accumulative roll bonding process. *Mater. Res. Express* **2019**, *6*, 96503. [[CrossRef](#)]
27. Dreizin, E.L. Metal-based reactive nanomaterials. *Prog. Energy Combust. Sci.* **2009**, *35*, 141–167. [[CrossRef](#)]
28. Ligachev, A.E.; Potemkin, G.V.; Lepakova, O.K.; Zhidkov, M.V.; Teresov, A.D.; Golobokov, N.N.; Maksimov, Y.M.; Kolobov, Y.R.; Koval, N.N. Ignition of a Ti-Al-C System by an Electron Beam. *Combust. Explo. Shock Waves* **2018**, *54*, 158–164. [[CrossRef](#)]
29. Fritz, G.M.; Grzyb, J.A.; Knio, O.M.; Grapes, M.D.; Weihs, T.P. Characterizing solid-state ignition of runaway chemical reactions in Ni-Al nanoscale multilayers under uniform heating. *J. Appl. Phys.* **2015**, *118*, 135101. [[CrossRef](#)]
30. Morsi, K. Review: Reaction synthesis processing of Ni-Al intermetallic materials. *Mater. Sci. Eng. A* **2001**, *299*, 1–15. [[CrossRef](#)]
31. Manukyan, K.V.; Mason, B.A.; Groven, L.J.; Lin, Y.; Cherukara, M.; Son, S.F.; Strachan, A.; Mukasyan, A.S. Tailored Reactivity of Ni+Al Nanocomposites: Microstructural Correlations. *J. Phys. Chem. C* **2012**, *116*, 21027–21038. [[CrossRef](#)]
32. Reeves, R.V.; Mukasyan, A.S.; Son, S.F. Thermal and Impact Reaction Initiation in Ni/Al Heterogeneous Reactive Systems. *J. Phys. Chem. C* **2010**, *114*, 14772–14780. [[CrossRef](#)]
33. Shuck, C.E.; Mukasyan, A.S. Reactive Ni/Al Nanocomposites: Structural Characteristics and Activation Energy. *J. Phys. Chem. A* **2017**, *121*, 1175–1181. [[CrossRef](#)] [[PubMed](#)]
34. Zhou, Q.; Hu, Q.; Wang, B.; Zhou, B.; Chen, P.; Liu, R. Fabrication and characterization of the Ni–Al energetic structural material with high energy density and mechanical properties. *J. Alloys Compd.* **2020**, *832*, 154894. [[CrossRef](#)]

35. Wang, P.; Xu, D.X.; Cheng, D.F.; Li, Q.; Niu, J.T. Active brazing filler metal on SiC particle reinforced aluminium matrix composites. *Sci. Technol. Weld. Join.* **2015**, *20*, 361–370. [[CrossRef](#)]
36. Feng, G.; Li, Z.; Zhou, Z.; Yang, Y.; Sekulic, D.P.; Zachariah, M.R. Microstructure and mechanical properties of C_f/Al-TiAl laser-assisted brazed joint. *J. Mater. Process. Technol.* **2018**, *255*, 195–203. [[CrossRef](#)]